

# Effective Hamiltonian approach to the Quantum Phase transitions in the extended Jaynes-Cummings model

H. T. Cui <sup>1,\*</sup> Y. A. Yan <sup>1,†</sup> M. Qin <sup>1,‡</sup> and X. X. Yi <sup>2,§</sup>

<sup>1</sup> *School of Physics and Optoelectronic Engineering & Institute of Theoretical Physics, Ludong University, Yantai 264025, China and*

<sup>2</sup> *Center for Quantum Sciences, Northeast Normal University, Changchun 130024, China*  
(Dated: December 12, 2023)

The study of phase transitions in dissipative quantum systems based on the Liouvillian is often hindered by the difficulty of constructing a time-local master equation when the system-environment coupling is strong. To address this issue, the complex discretization approximation for the environment has been proposed to study the quantum phase transition in the extended Jaynes-Cummings model with an infinite number of boson modes. This approach yields a non-Hermitian effective Hamiltonian that can be used to simulate the dynamics of the spin. It was found that the ground state of this effective Hamiltonian determines the spin dynamics in the single-excitation subspace. Depending on the opening of the energy gap and the maximum population of excitations on the spin degree of freedom, three distinct phases can be identified: fast decaying, localized, and stretched dynamics of the spin. This approach can be extended to multiple excitations, and similar dynamics were found in the double-excitation subspace, indicating the robustness of the single-excitation phase.

Keywords:

## I. INTRODUCTION

The study of open quantum systems has revealed that phase transitions can occur, even though the system has a finite number of degrees of freedom [1]. Unlike the phase transitions in closed systems under thermodynamic conditions, the phase transitions in open quantum systems are accompanied by significant changes in the system's dissipative dynamics. Thus, the so called dissipative phase transition (DPT) reflects the non-equilibrium of system and the nontrivial properties of steady state of the system. Moreover by environment engineering, one can prepare the system in a special state through DPT, that would be difficult or impossible by conventional ways [2]. To characterize DPT explicitly, the system's Liouvillian eigenvalues is studied, of which the real part corresponds to the decay rate of eigenmodes [3]. It was noted that the vanishing of the gap in the excitation spectrum of Liouvillian indicates a non-analytical change in the dissipative dynamics of system, which typically signals the onset of a phase transition [3].

Recent experimental advances have allowed physicists to investigate regimes beyond Markovian approximation, such as in solid-state [4] and artificial light-matter systems [5]. In this situation, the Liouvillian is difficult to determine due to the memory effect of environment. This raise the question of whether phase transitions can still be found in the absence of a Liouvillian and if so, how to characterize it explicitly. To address this, the method

of perturbational expansion or numerical simulation has been used to incorporate the influence of environment [6]. However, the resulting dynamical equations are often very complicated, making it difficult to determine the phase transition [7]. An alternative approach is to approximate the environment as a many-body system with discrete and finite energy modes. Thus, an effective Hamiltonian can be constructed to predicate the dynamics of system [8, 9]. However, this approach requires a large Hilbert space dimension to accurately predicate the long-term behavior of system, which would become unaffordable in computation. To surmount this difficulty, a complex discretization approximation for environment was proposed by the authors [10], which allows for a more efficient computation and more faithful depiction of the dissipative dynamics of system by introducing an effective Hamiltonian. Thanking to the non-Hermiticity of effective Hamiltonian, the decay rate of eigenmode can be characterized by the imaginary part of corresponding eigenvalue.

The similarity of the Liouvillian and the effective Hamiltonian encourages us to explore the phase transition by solving the complex Hamiltonian. This approach incorporates the dynamical information for both the system and environment. So by studying the eigenvalues and corresponding eigenvectors, one can gain the deep insight into the dynamics of system. As an illustration, the extended Jaynes-Cummings model is discussed in this paper. This model is the generalization of the spin-boson model under rotating-wave approximation. It was known that the spin-boson model undergoes a quantum phase transition in the sub-Ohmic or Ohmic regime from a delocalized phase with a single ground state and no magnetization, to a localized phase with two-fold degenerate ground state and a nonzero magnetization [11]. However, the nonpreservation of total excitations in the spin-

\*Electronic address: cuiht01335@aliyun.com

†Electronic address: yunan@ldu.edu.cn

‡Electronic address: qinming@ldu.edu.cn

§Electronic address: yixx@nenu.edu.cn

boson model makes the investigation of the phase transition complicated [12]. The rotating-wave approximation is a reasonable choice to obtain tractable solutions [7]. Furthermore, it allows us to determine the phase transition by finding singularity of order parameter. A similar research has been performed in Ref. [13], where the effective Hamiltonian is constructed in real space. Thus, the magnetization  $\langle\sigma_z\rangle$  and  $\langle\sigma_x\rangle$  are evaluated for the ground state to detect phase transitions.

In contrast, a non-Hermitian effective Hamiltonian is constructed in this paper to determine the phase transition in the single-excitation subspace of extended Jaynes-Cumming model. Because of the non-Hermiticity, the eigenvalue of effective Hamiltonian shows the imaginary part, which characterizes the decaying dynamics of spin. Importantly, besides of the known decaying phase and localization phase [14], the intermediate phase can be verified through checking the ground state function. The intermediate phase demonstrates stretched-like behavior in dynamics. By our knowledge, it is the first time for the identification of this phase in the extended Jaynes-Cumming model. Moreover, the approach can be readily extended into the multi-excitation subspace. As a result, we explore the spin dynamics in the double-excitation subspace by exact digitalization method. Interestingly, the spin dynamics in this case could shows the similar behavior as that in single-excitation subspace, which implies that the single-excitation phases would be stable.

The remaining of the paper is organized as follows. The model and method are introduced in Section II, with particular remarks on the complex discretization approximation for environment. In section III, the spin dynamics is discussed explicitly in the single-excitation subspace by solving the effective complex Hamiltonian. Resultantly, a phase diagram is founded. In section IV, we extend the discussion into the double-excitation subspace. It is found that the spin dynamics in this case is nearly the same as in single-excitation subspace. Finally, conclusions are offered in section V.

## II. MODEL AND METHOD

In this section, we introduce the model and present the overview of complex discretization approximation.

### A. Extended Jaynes-Cumming model with infinite number of boson modes

Its Hamiltonian can be written as

$$H = \Delta\sigma_+\sigma_- + \sum_k \omega_k a_k^\dagger a_k + \sum_k \left( g_k a_k^\dagger \sigma_- + g_k^* a_k \sigma_+ \right). \quad (1)$$

where  $\sigma_\pm = (\sigma_x \pm i\sigma_y)/2$  with  $\sigma_i (i = x, y, z)$  the Pauli matrices and  $i$  is the imaginary unit.  $a_k^\dagger (a_k)$  denotes the creation (annihilation) operator of mode  $k$  in environment, which is coupled to the spin via coupling strength

$g_k$ . In this paper, the spectral density for environment is chosen as

$$J(\omega) = \sum_k |g_k|^2 \delta(\omega - \omega_k) = \eta \omega \left( \frac{\omega}{\omega_c} \right)^{s-1} e^{-\omega/\omega_c}, \quad (2)$$

where  $\eta$  depicts the coupling strength, and  $\omega_c$  is the cut-off of frequency. Depending the value of  $s$ , the environment is classified as sub-Ohmic ( $0 < s < 1$ ), Ohmic ( $s = 1$ ) and super-Ohmic ( $s > 1$ ). Although the simplicity of Eq. (1), the exact spin dynamics can be obtained only in the single-excitation subspace. In this case, the state of total system can be written as

$$|\psi(t)\rangle = \alpha(t)|e\rangle|0\rangle^{\otimes N} + |g\rangle \left( \sum_k \beta_k(t)|1\rangle_k \right), \quad (3)$$

in which  $N$  denotes the number of modes in environment,  $|1\rangle_k = a_k^\dagger|0\rangle_k$  with the vacuum state  $|0\rangle_k$ , and  $|e\rangle = \sigma_+|g\rangle$ . Substituting Eq. (3) into the Schrödinger equation, one gets

$$i \frac{\partial}{\partial t} \alpha(t) = \Delta \alpha(t) - i \int_0^t d\tau \alpha(\tau) \int_0^\infty d\omega J(\omega) e^{-i\omega(t-\tau)} \mathbb{1}$$

where the last term stems from the memory effect of environment.

It was known that the spin dynamics in the single-excitation subspace can display the transition from decaying to localization because of the occurrence of bound state [14, 15]. The bound state corresponds to a singular energy level, separated from the continuum of environment. The existence of bound states can be verified by solving Eq. (4) [14]. By Laplace transformation, Eq. (4) can be rewritten as

$$\alpha(p) = \left[ i\Delta + p + i \int_0^\infty d\omega \frac{J(\omega)}{ip - \omega} \right]^{-1}, \quad (5)$$

where  $\alpha(p) = \int_0^\infty e^{-pt} \alpha(t) dt$ . If  $p = -iE$  satisfying the equation

$$\Delta - E - \int_0^\infty d\omega \frac{J(\omega)}{E - \omega} = 0, \quad (6)$$

one then obtains  $\alpha(t) \propto e^{-iEt}$  by inverse Laplace transformation. This feature means that the modulus of  $\alpha(t)$  may be constant, leading to localization in the dynamics. The real solution to Eq. (6) can be found in the regime of  $E < 0$ , depending on  $J(\omega)$  [15]. Moreover, since  $\omega_k \in [0, \infty)$ , the bound state can be viewed as the ground state of total system. In this sense, the transition is a result of the opening of energy gap of ground state from the continuum.

Eq. (4) can be solved using iterative method, but the memory effect renders the calculation time-consuming

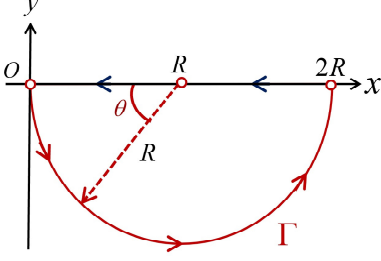


Figure 1: (Color online) Illustration of the path in complex plane used to approximate  $\int_0^\infty dx$  as  $\int_\Gamma dz$ , where  $\Gamma$  denotes the semi-circle with radius  $R$ , centered at  $(R, 0)$ .

exhaustive for long term evolution. For multiple excitations, the lack of a dynamical equation similar to Eq. (4) renders it difficult to analyze the spin dynamics and determine the bound state [16]. To address this, a feasible approach is to discretize the environment into a finite set of modes, thereby constructing an effective Hamiltonian that can be solved with exact diagonalization [9]. However, this approach suffers from the recurrence caused by the finite dimension, which make the evaluation unaffordable for long term evolution.

### B. Complex discretization approximation

Recently, the complex discretization approximation (CDA) method has been introduced to refine the simulation of spin dynamics [10]. In contrast to its counterpart in real space [9], this method yields a non-Hermitian effective Hamiltonian  $H_{\text{dis}}$ , which has complex eigenvalues with a negative imaginary part. Consequently,  $H_{\text{dis}}$  can provide more accurate description of the dissipative dynamics of spin.

The discretization approximation was proposed to tackle the infinite energy modes in environment by utilizing the Gauss quadrature [9]. For this purpose, Eq. (1) is transformed under the continuous limit as [17],

$$H = \Delta \sigma_+ \sigma_- + \int_0^\infty dx h(x) a_x^\dagger a_x + \int_0^\infty dx [g(x) a_x^\dagger \sigma_- + g^*(x) a_x \sigma_+]. \quad (7)$$

The operator  $a_x$  or  $a_x^\dagger$  fulfill the bosonic commutation relation  $[a_x^\dagger, a_{x'}] = \delta(x - x')$ . The spectral function  $J(\omega)$  can be rewritten for variable  $x$  as [17]

$$J(x) = g^2 [h^{-1}(x)] \frac{dh^{-1}(x)}{dx}. \quad (8)$$

The equivalence between Eq. (1) and Eq. (7) is guaranteed by the fact that the same effective action for spin degree of freedom can be derived from the Hamiltonians Eq. (1) and Eq. (7) [17].

It is noteworthy that the forms of  $h(x)$  or  $g(x)$  are not uniquely determined for a given  $J(x)$ . By this freedom,

one can choose proper form for  $h(x)$  or  $g(x)$  for the sake of discretization of environment [9]. Given Ohmic spectral function Eq. (2), one may choose

$$h(x) = \omega_c x, g(x) = \sqrt{\eta} \omega_c x^{s/2} e^{-x/2}. \quad (9)$$

Assuming that  $h(x)$  has a linear relationship with variable  $x$  is beneficial to the discretization approximation for environment.

The main idea of CDA is to utilize complex Gauss quadratures to discretize continuum of the environment. For this purpose,  $\int_0^\infty dx$  is replaced by a line integral  $\int_\Gamma dz$  in complex plane shown in Fig. 1, where  $z = x + iy$ .  $\Gamma$  denotes the semi-circle with radius  $R$  in the lower half complex plane, centered at  $(R, 0)$ . With the requirement that both  $h(x)$  and  $g(x)$  have no singularity in complex plane,  $\int_\Gamma dz$  is equal to  $\int_0^\infty dx$  by Cauchy theorem if  $R \rightarrow \infty$ . Along the path  $\Gamma$ ,  $z = R(1 + e^{i\theta})$  with  $\theta \in [\pi, 2\pi]$ . Thus, the real part of  $z$  is ensured to be nonnegative, characterizing the energy mode in environment. The value of  $R$  is responsible for the effective energy modes in environment, used to simulate the spin dynamics.

Similar to the way in [9], the following transformation is introduced

$$\begin{aligned} d_n &= \int_\Gamma dz \sqrt{\frac{w(z)}{iz}} \eta_n(z) a_z \\ d_n^\dagger &= \int_\Gamma dz \sqrt{\frac{w(z)}{iz}} \eta_n(z) a_z^\dagger \end{aligned} \quad (10)$$

and the inverse

$$\begin{aligned} a_z &= \sqrt{\frac{w(z)}{iz}} \sum_{n=0}^{N-1} \eta_n(z) d_n \\ a_z^\dagger &= \sqrt{\frac{w(z)}{iz}} \sum_{n=0}^{N-1} \eta_n(z) d_n^\dagger, \end{aligned} \quad (11)$$

where  $a_z^\dagger(a_z)$  is the complex generalization of  $a_x^\dagger(a_x)$ . It is natural to require the invariance of bosonic commutation relation, i.e.  $[a_z^\dagger, a_{z'}] = \delta(z - z')$ .  $\eta_n(z)$  denotes the polynomial of degree  $n$ , which can be constructed through the inner product with respect to weight function  $w(z)$ ,

$$\langle f, g \rangle_\Gamma = \int_\Gamma \frac{dz}{iz} w(z) f(z) g(z). \quad (12)$$

It is stressed that the inner product is defined deliberately without complex conjugation to construct the three-term recurrence relation for  $\eta_n(z)$  [18]. By this way,  $\eta_n(z)$  can display two features, which are crucial for discretization of Eq. 7. One is the orthonormality defined as

$$\langle \eta_m, \eta_n \rangle_\Gamma = \delta_{m,n}. \quad (13)$$

The other is the recurrence relation

$$\sqrt{\nu_{n+1}} \eta_{n+1}(z) = (z - i\mu_n) \eta_n(z) - \sqrt{\nu_n} \eta_{n-1}(z), \quad (14)$$

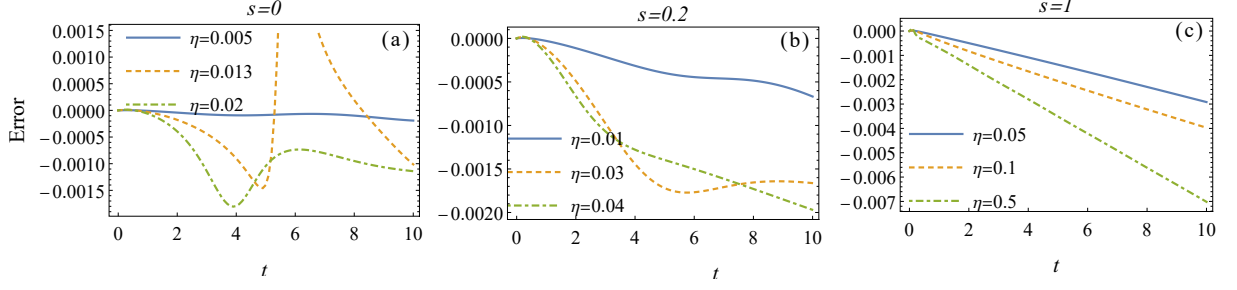


Figure 2: (Color online) The plots for the computational errors defined in Eq. (21). For all plots,  $N = 2000$ ,  $R = 6$ ,  $\Delta = 1$ , and  $\omega_c = 10$  are chosen.

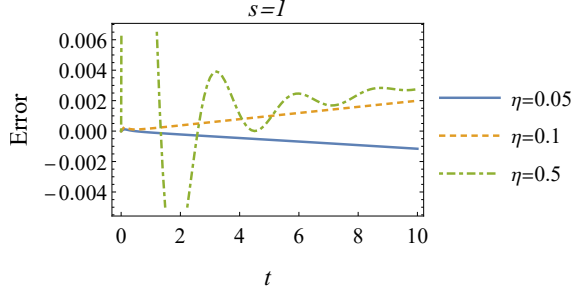


Figure 3: (Color online) The plot for the computational errors when  $\tilde{H}_{\text{dis}}$  is used to evaluate the survival probability for  $s = 1$ . It is stressed that the data for  $\eta = 0.05$  and  $0.1$  has been enlarged by ten times in convenience of illustration. The other parameters are the same as those in Fig. 2.

where

$$i\mu_n = \langle z\eta_n, \eta_n \rangle_\Gamma, \nu_n = \frac{A_{n-1}^2}{A_n^2}, \quad (15)$$

$A_n$  being the coefficient of  $z^n$  in  $\eta_n(z)$ . With help of these two properties and transformation Eq. (11) together, Eq.(7) can be transformed into the following form

$$H = \Delta\sigma_+\sigma_- + \omega_c \sum_{n=1}^N (i\mu_n d_n^\dagger d_n + \sqrt{\nu_n} d_n^\dagger d_{n-1} + \text{h. c.}) + \sum_{n=1}^N \int_\Gamma dz \sqrt{\frac{w(z)}{iz}} \eta_n(z) [g(z)\sigma_+ d_n + g^*(z)d_n^\dagger \sigma_-], \quad (16)$$

where  $N$  is the highest degree of polynomial, used in the evaluation.  $h(z)$  and  $g(z)$  can be obtained directly through replacing  $x$  in Eq. (9) by  $z$ .

As further simplification, let introduce the new mode operator

$$\begin{aligned} \tilde{d}_i &= \sqrt{w_i} \sum_{n=1}^N \eta_n(z_i) d_n, \\ \tilde{d}_i^\dagger &= \sqrt{w_i} \sum_{n=1}^N \eta_n(z_i) d_n^\dagger, \end{aligned} \quad (17)$$

where  $z_i$  denotes the root of  $\eta_N(z)$ , and  $w_i$  is the corresponding weight. Both  $z_i$  and  $w_i$  can be obtained by diagonalizing the second term in Eq. (16). For the last term in Eq. (16), the integration can be approximated by complex Gauss quadrature [18] as

$$\begin{aligned} \int_\Gamma dz \sqrt{\frac{w(z)}{iz}} \eta_n(z) g(z) &= \int_\Gamma dz \frac{w(z)}{iz} \sqrt{\frac{iz}{w(z)}} \eta_n(z) g(z) \\ &\simeq \sum_{i=1}^N \sqrt{\frac{iz_i}{w(z_i)}} w_i \eta_n(z_i) g(z_i) \end{aligned} \quad (18)$$

Together with Eqs.(17), one finally obtains

$$H_{\text{dis}} = \Delta\sigma_+\sigma_- + \sum_{i=1}^N z_i \tilde{d}_i^\dagger \tilde{d}_i + \sum_{i=1}^N (g_i \sigma_+ \tilde{d}_i + \text{h.c.}) \quad (19)$$

where  $g_i = \sqrt{\frac{iz_i}{w(z_i)}} \sqrt{w_i} g(z_i)$ .

Obviously,  $H_{\text{dis}}$  is non-Hermitian, and the evolution operator can be written as [21]

$$U(t) = \sum_n e^{-i\mathbb{E}_n t} |n\rangle_R \langle n|, \quad (20)$$

where  $|n\rangle_R$  denotes the right eigenfunction of  $H_{\text{eff}}$  with eigenvalue  $\mathbb{E}_n$ , and  $|n\rangle_L$  denotes the left eigenfunction with eigenvalue  $\mathbb{E}_n^*$ . As an exemplification, the survival probability  $|\langle \psi(t) | \psi(0) \rangle|^2$  with  $|\psi(0)\rangle = |e\rangle|0\rangle^{\otimes N}$  is explored respectively by exact solution of Eq. (4) and CDA. The computational error, defined as

$$\text{Error} = \frac{\text{CDA} - \text{Exact}}{\text{CDA} + \text{Exact}}, \quad (21)$$

is presented in Fig. 2 for different values of  $s$  and  $\eta$  (the explicit plots for the evolution of survival probability are provided by Fig.A1 in Appendix I). Nonetheless, due to the time-consuming nature of solving Eq. (4), the exact evaluation are restricted up to  $t = 10$  with the step length of  $10^{-4}$ . For CDA, the weight function chosen is  $w(z) = 1$ , which might cause the appearance of complex eigenmodes in the environment. It should be stressed that choosing  $g(z)$  as the weight function will not generate a non-Hermitian effective Hamiltonian. Evidently,

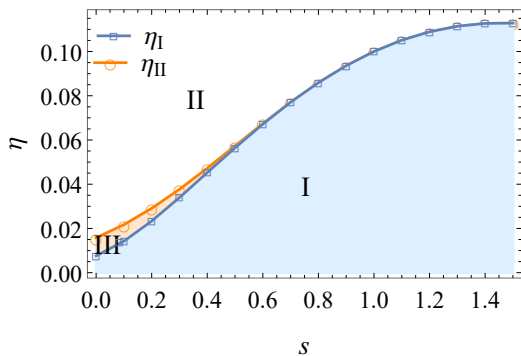


Figure 4: (Color online) The phase diagram for  $H_{\text{dis}}$  in the single-excitation subspace. All points are determined by exact diagonalization of  $H_{\text{dis}}$ . Region I: delocalized phase. Region II: localized phase. Region III: intermediate phase.  $\eta_I$  denotes the critical value, where the energy gap is zero.  $\eta_{II}$  denotes the critical value, where the imaginary part of ground state function on basis state  $|e\rangle|0\rangle^{\otimes k}$  is zero. For this plot,  $R = 6$ ,  $N = 1000$  and  $\Delta = 1, \omega_c = 10$  are chosen.

the computational errors has a magnitude of  $10^{-3}$  in most circumstances, and thus CDA can provides reliable evaluation of spin dynamics.

However, Fig. 2(c) shows a significant increase of error when  $s = 1$ . The explicit calculations reveals a slow convergence to stable result as  $N$  increases. To capture the long-term behavior of spin dynamics, we propose to use

$$\tilde{H}_{\text{dis}} = \sqrt{H_{\text{dis}}^\dagger \cdot H_{\text{dis}}}. \quad (22)$$

as an evaluation. This is because  $H_{\text{dis}}^\dagger$  would creat a gain effect since its complex eigenvalues have a positive imaginary part, which is expected to reduce the errors. To justify this proposition, we reexamine the spin dynamics of  $s = 1$  by  $\tilde{H}_{\text{dis}}$ . As shown in Fig. 3,  $\tilde{H}_{\text{dis}}$  provides a reliable assessment of  $|\langle\psi(t)|\psi(0)\rangle|^2$  for  $\eta = 0.05$  and  $0.1$ , with a significant reduction of error by at least a factor of ten. The explicit illustration for the evolution can be found in Fig. A2 in Appendix I

For  $\eta = 0.5$ . the evaluation of  $\tilde{H}_{\text{dis}}$  is reliable only for larger  $t$ , however it becomes very poor for  $t < 3$ , as shown in Fig. A2(c). Therefor, we use  $H_{\text{dis}}$  for spin dynamics evaluation for times shorter than  $\sim 4$  and  $\tilde{H}_{\text{dis}}$  for times greater than 4. It is important to note that  $H_{\text{dis}}$  is only applicable when  $s = 1$ , whereas  $H_{\text{dis}}$  can provide reliable results for  $s = 0$  and  $0.2$ .

### III. QUANTUM PHASE TRANSITION IN THE SINGLE-EXCITATION SUBSPACE

Actually, the CDA method transforms the open quantum system into a closed many-body system, allowing for the conventional approach to quantum phase transition [19] to be applied. An overview to the main result

of this section is provided first. After then, the spectrum of  $H_{\text{dis}}$  is studied, with a focus on the energy gap of ground state, which can be used to identify the quantum phase transition. Finally, the ground state function is analyzed in details, which shows a significant change in the population of excitation with an increase of the coupling strength  $\eta$  and thus indicates an intrinsic transition of spin dynamics.

#### A. overview to the main result

The main result is summarized as the phase diagram shown in Fig. 4. Evidently, phase diagram can ge divided into three regions, labelled as I, II and III. The region I denotes the dissipative phase, where the spin dynamics decay rapidly and excitation is absorbed into environment. In contrast, the region II denotes the localized phase, where excitation may be localized in spin system by a finite probability. Between this two regions, a third region, named as Phase III, can be found for small  $s$ . In this region, the spin dynamics shows an intermediate behavior between the fast decaying and localization. Our calculation shows that the dynamics of system in this region displays an stretched-like feature. This feature is a result of the competition of the dissipation induced by coupling to environment and the localization from the opening of energy gap of ground state. The boundary between region I and II or III is decided by critical value  $\eta_I$  or  $\eta_{II}$ . At  $\eta_I$ , the energy gap of ground state opens, while at  $\eta_{II}$  the population of excitation of the ground state becomes maximal in the spin degree of freedom. For large  $s$ ,  $\eta_I$  and  $\eta_{II}$  merge into a single one, at which the spin dynamics shows an intermediate feature. The relevance of  $\eta_I$  and  $\eta_{II}$  to  $N$  and  $R$  is studied in Appendix II

The survival probability  $|\langle\psi(t)|\psi(0)\rangle|^2$  with  $|\psi(0)\rangle = |1\rangle|0\rangle^{\otimes k}$  is evaluated to illustrate the distinct dynamics in three regions. As shown in Fig. 5, dependent on the values of  $s$  and  $\eta$  belonging to different regions in Fig. 4,  $|\langle\psi(t)|\psi(0)\rangle|^2$  can display fast decaying and localization respectively. In order to display the intermediate dynamics in region III, a numerical fitting for the long-term evolution of  $|\langle\psi(t)|\psi(0)\rangle|^2$  is provided in Fig. A4 in Appendix II, based on the fitting function  $B \exp(-At^\beta)$ . It is found that the exponential index  $\beta$  has the magnitude of order  $10^{-1}$ , which clearly demonstrate the stretched-like feature of the evolution.

#### B. The spectrum of $H_{\text{dis}}$

To understand the phase diagram, the spectrum of  $H_{\text{dis}}$  is studied in this subsection, obtained by exactly diagonalizing  $H_{\text{dis}}$ . As shown in Fig. 6, the eigenvalues exhibit a non-positive imaginary part, characterizing the dissipative spin dynamics. Furthermore, their real parts are confined at interval  $(0, 120)$ . This is a consequence

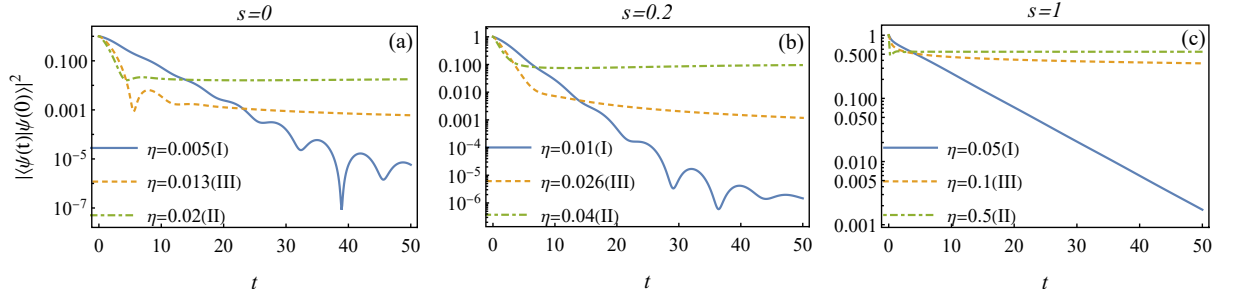


Figure 5: (Color online) The evolution of survival probability is plotted for selected  $s$  and  $\eta$ . For panels (a) and (b), the evolution is obtained by  $H_{\text{dis}}$ . While for panel (c),  $\tilde{H}_{\text{dis}}$  is used to obtain convergent results for  $\eta = 0.05, 0.1$ . As for  $\eta = 0.5$ , the evolution is determined by the combination of  $H_{\text{dis}}$  and  $\tilde{H}_{\text{dis}}$ , as stated at the end of II B. The Roman numbers denote the different regions in Fig. 4, to which the chosen values of  $s$  and  $\eta$  belong. For all plots,  $N = 2000$ ,  $R = 6$ ,  $\Delta = 1$ , and  $\omega_c = 10$  are chosen.

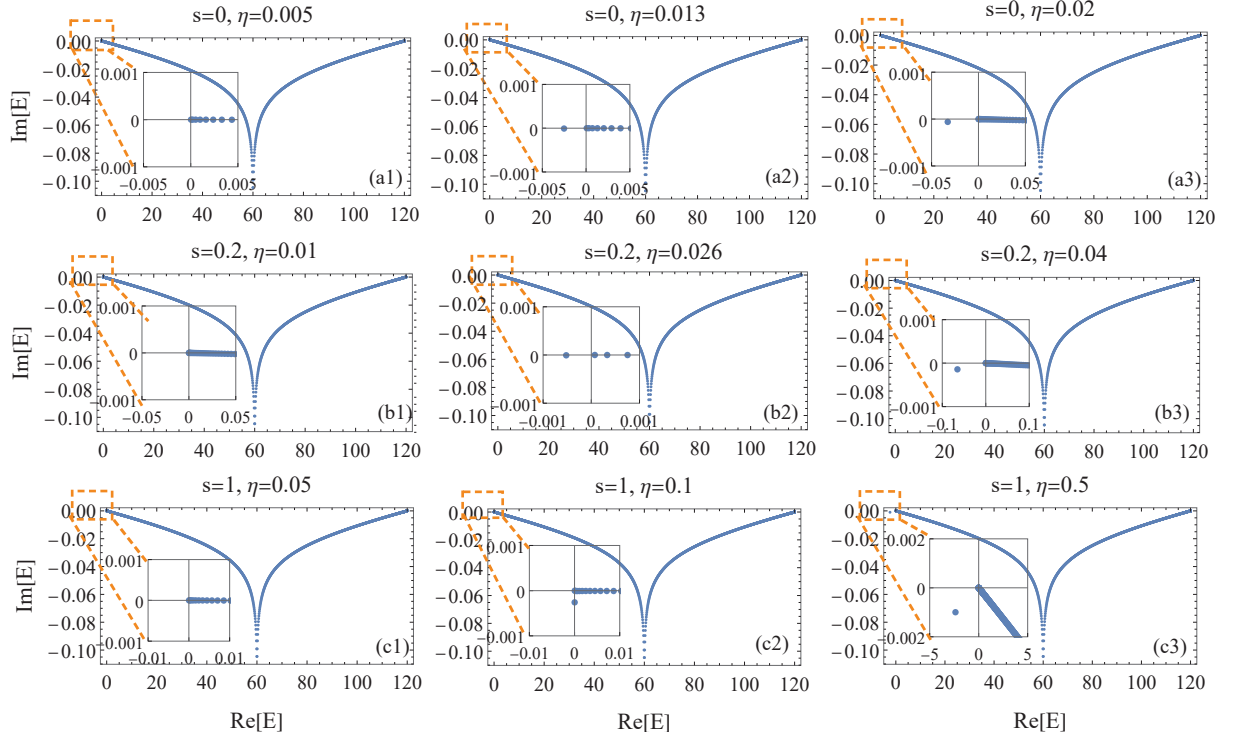


Figure 6: (Color online) Plots of the spectrum of  $H_{\text{dis}}$  for different  $s$  and  $\eta$ . For all plots,  $N = 2000$ ,  $R = 6$ ,  $\Delta = 1$ , and  $\omega_c = 10$  are chosen.

of CDA approach, that the continuum of environment may be discretized as a finite spectrum bound at interval  $(0, 2R\omega_c)$ .

As for the non-Hermiticity of  $H_{\text{dis}}$ , the ground state can be defined as the right eigenfunction with the minimal real part of its eigenvalue. For small  $\eta$ , the ground state would correspond to the energy level with the real part close to zero, as shown by left column in Fig. 6. However when  $\eta$  increases beyond a critical value  $\eta_I$  related to  $s$ , a single level emerges in the region  $\Re[E] < 0$ , as shown by the middle and right columns in Fig. 6. In this case, the ground state becomes separated from the level band by a energy gap, which is equal to the real part of its

eigenvalue. In addition, the gap increases with increment of  $\eta$ .

Physically, the single ground state corresponds to the photon-bound state, which has been known to be associated with the localized dynamics of system [14, 15]. Nevertheless, as shown in Fig. 5, the opening of energy gap does not guarantee the emergence of localization in the dynamics, a stretched-like decaying observed when  $\eta > \eta_I$ . Additionally, localized dynamics can only be observed when  $\eta$  surpasses a second critical value. Consequently, to understand the intricate behaviors, it is necessary to inspect the ground state function.



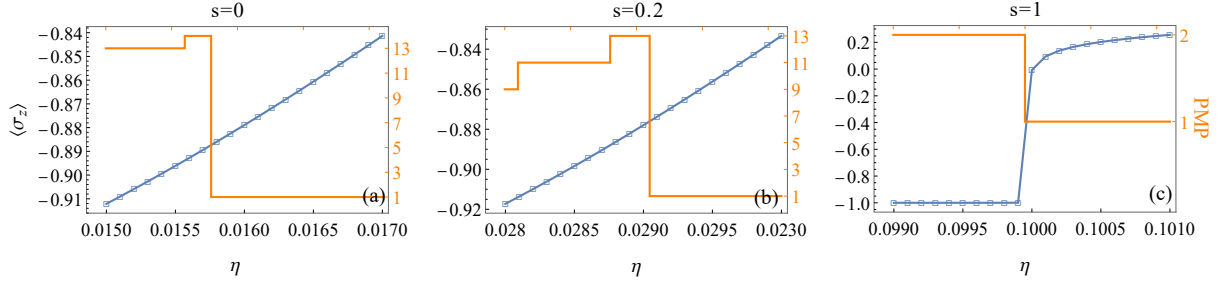


Figure 7: (Color online) The PMP(orange line) and average value of  $\sigma_z$  (blue line) for the ground state of  $H_{\text{dis}}$  vs.  $\eta$ . For P.M.P., the arabic numbers denote the basis state  $|k\rangle$ . The parameters are chosen the same in Fig. 6

### C. The ground state function

The ground state function can be obtained directly by solving  $H_{\text{dis}}$ , which can be written formally as  $|g\rangle = \alpha|e\rangle|0\rangle + |g\rangle(\sum_k \beta_k(t)|1\rangle_k)$ . Here,  $|e\rangle|0\rangle \equiv |1\rangle$  denotes excitation in the spin, while  $|g\rangle|1\rangle_k \equiv |k\rangle$  ( $k = 2, 3, \dots, N+1$ ) denotes the excitation in the  $k$ -th mode of environment. The population of excitation on  $|1\rangle$  has a significant influence on the localized evolution of  $|\langle\psi(t)|\psi(0)\rangle|^2$ . In Fig.7, the position of maximal population (PMP) on the basis state  $|k\rangle$  is explored for the ground state when  $s = 0, 0.2$  and  $1$ . For the three situations, the energy gap of ground state opens at critical point  $\eta_I = 0.0076, 0.02335$  and  $0.1$  respectively, as illustrated in Fig.4. However, as shown in Fig. 7 (a) and (b), PMP at  $|1\rangle$  can happen only when  $\eta$  is beyond a critical value, labeled as  $\eta_{II}$ . This can explain the evolution illustrated in Fig. 5(a) and (b), in which the localized behavior of  $|\langle\psi(t)|\psi(0)\rangle|^2$  can occur only for  $\eta$  considerably greater than  $\eta_I$ . Thus, the stretched-like dynamics is a result of the competition between the energy gap, which protects excitation against the spontaneous emission into environment, and the intrinsic dissipation in the ground state function, which does not support PMP at  $|1\rangle$ .

For  $s = 1$ ,  $\eta_{II}$  is found to be almost equal to  $\eta_I$ . Thus, the stretched-like evolution can be found at critical point  $\eta_I = 0.1$ . Additionally, Fig. A5 (c) in Appendix II reveals that  $\eta_{II}$  is smaller than  $\eta_I$ . This difference, however, tends to diminish when  $N \rightarrow \infty$ . Similar picture can also be found for other values of  $s$ .

In addition, the average value  $\langle\sigma_z\rangle$  for the ground state is evaluated in order to detect phase transition. As shown by Fig. 5,  $\langle\sigma_z\rangle$  remains continuous for  $s = 0, 0.2$ , yet a jump is observed at  $\eta = 0.1$  for  $s = 1$ , implying that the transition for  $s = 1$  may be distinct from  $s = 0, 0.1$ .

Conclusively, we have demonstrated the presence of a second critical point  $\eta_{II}$  by analyzing the ground state function. For small  $s$ ,  $\eta_{II}$  is distinct from  $\eta_I$ , and an intermediate region can be identified where the spin dynamics shows stretched-like behavior. As  $s$  increases,  $\eta_{II}$  tends to be equal to  $\eta_I$ , and the stretched-like spin dynamics can happen at critical point. Furthermore, the two scenarios can be distinguished by evaluating  $\langle\sigma_z\rangle$  for the ground state. If  $\eta_{II}$  not equal to  $\eta_I$ ,  $\langle\sigma_z\rangle$  is contin-

uous at  $\eta_{II}$ . Conversely, If  $\eta_{II}$  tends to be equal to  $\eta_I$ ,  $\langle\sigma_z\rangle$  exhibits a jump c at  $\eta_{II}$ .

### IV. SPIN DYNAMICS IN THE DOUBLE-EXCITATION SUBSPACE

In the case of multiple excitations, the spin dynamics is difficult to study due to the absence of a compact equation similar to Eq. (4). CDA, however, provides an efficient approach to this issue. In principle, the dynamics can be obtained by exactly diagonalizing  $H_{\text{dis}}$  in the multiple excitation space. However, the dimension of  $H_{\text{dis}}$  increase drastically as the number of excitations, making the exact treatment highly demanding. Therefore, this section focuses only on the spin dynamics in the double-excitation subspace.

The wave function in the double-excitation subspace can be expressed as

$$|\phi(t)\rangle = |e\rangle \sum_{k=1}^N \alpha_k(t) a_k^\dagger |0\rangle^{\otimes N} + |g\rangle \sum_{k \leq k'} \beta_{k,k'}(t) a_k^\dagger a_{k'}^\dagger |0\rangle^{\otimes N} \quad (23)$$

Evidently,  $|e\rangle$  is correlated to the status of environment. To characterize the spin dynamics,

$$P_e(t) = \sum_{k=1}^N |\alpha_k(t)|^2. \quad (24)$$

is evaluated for arbitrary time  $t$ , which denotes the probability of the single excitation saved by the spin. The initial state is chosen as  $|\phi(0)\rangle = 1/\sqrt{N}|e\rangle \sum_{k=1}^N a_k^\dagger |0\rangle^{\otimes N}$  to avoid the dependence on special mode in environment.  $N = 200$  is chosen for the simulation, which corresponds to the Hilbert space of dimension  $\sim 2.0 \times 10^5$ . For larger  $N$ , the calculation becomes too consumptive to implement. To offset the recurrence induced by finite  $N$ ,  $\tilde{H}_{\text{dis}}$  is used to find convergent  $P_e(t)$  in this evaluation, which is illustrated by empty circles in Fig. 8. Because of finite  $N$ , the calculation becomes fluctuated when  $t > \sim 10$ . For  $s = 1$ , the calculation shows a slow convergency, which induces strong fluctuation and large computational error.

It is observed that  $P_e(t)$  displays similar evolution as  $|\langle\psi(t)|\psi(0)\rangle|^2$  in single excitation subspace. This has

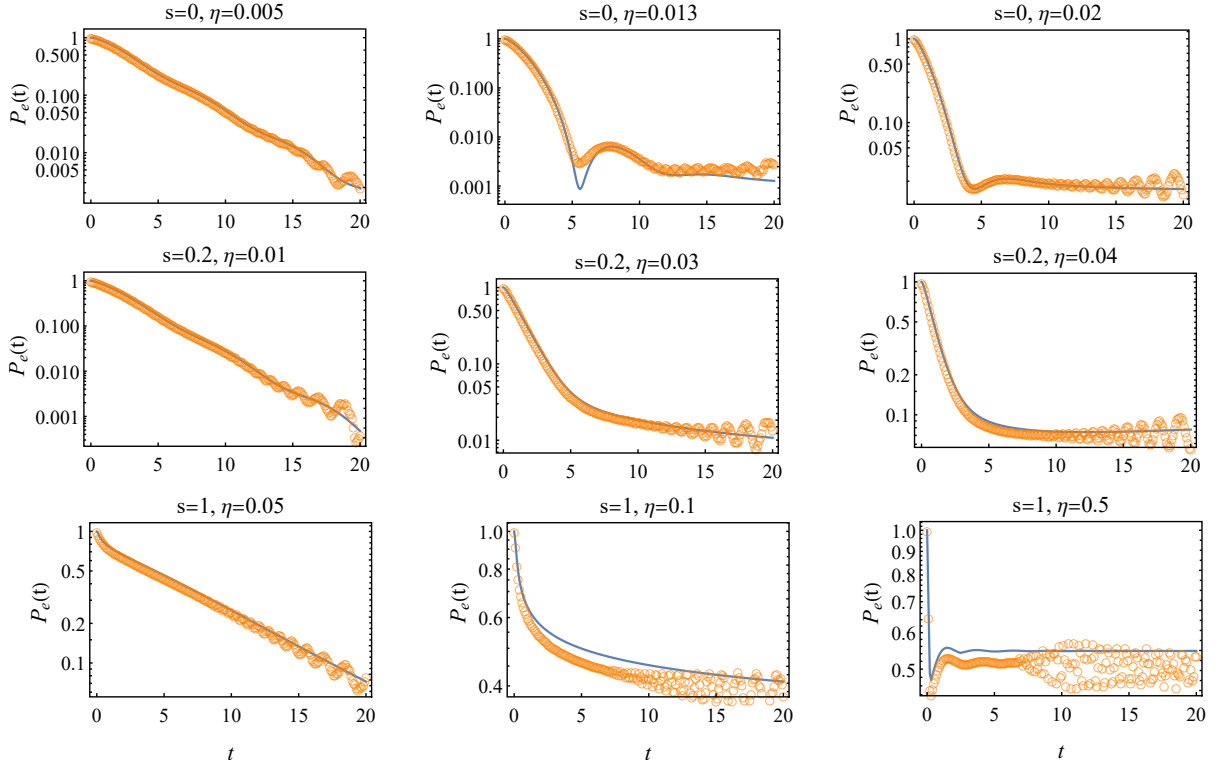


Figure 8: (Color online) The comparative plots of spin dynamics in the double-excitation subspace (empty circle) and single-excitation subspace (solid line). The spin dynamics in single-excitation subspace is evaluated by  $H_{\text{dis}}$  for  $s = 0, 0.2$  and  $\tilde{H}_{\text{dis}}$  for  $s = 1$ . For the calculation in double-excitation subspace,  $\tilde{H}_{\text{dis}}$  is solved by choosing  $N = 200$  in order to obtain the convergent result. For all plots,  $R = 6, \Delta = 1, \omega_c = 10$  are chosen.

been verified further by Gauss quadratures method in real space [9], as illustrated by Fig. A6 in Appendix III. This observation would be attributed to the fact that the discretized environment corresponds to an interaction-free bosonic system, in which the excitations can be populated freely at the mode of environment without any interference. Thus, the decay of excitation in spin would be independent of the status of environment. This implies that the phase diagram in single-excitation subspace would be robust against the increase of energy in the total system.

We try to find explanation of spin dynamics by analyzing spectrum of  $H_{\text{dis}}$ . However, the spectrum of  $H_{\text{dis}}$  does not provide sufficient evidence to explain the spin dynamics in terms of the ground state, as is possible in the single-excitation subspace. Calculations show that the energy gap can remain finite even when  $\eta < \eta_I$ , and the ground state can have positive energy in such cases. Furthermore, the number of eigenvalues with negative real parts depends on the value of  $\eta$ . Consequently, the bound state is absent in the multiple-excitation subspace, and the dynamics of spin cannot be explained from the single-excitation perspective.

## V. CONCLUSION

In conclusion, the quantum phases in the extended Jaynes-Cummings model was investigated in this paper. To simulate the open dynamics of spin, a non-Hermitian effective Hamiltonian  $H_{\text{dis}}$  was constructed using complex discretization approximation for the environment. The validity of this approach was confirmed by examining the spin dynamics in single-excitation subspace, which was determined exactly by solving Eq. 4. By exactly diagonalizing  $H_{\text{dis}}$ , the spin dynamics could be further examined by analyzing the ground state, which revealed eigenvalue with the smallest real part. It was found that the spin dynamics in single-excitation subspace is strongly related to two key properties of the ground state, the energy gap, defined as the negative real part of its eigenvalue, and PMP of ground state on the basis state. When the energy gap is zero, the spin dynamics, measured by the survival probability of initial state  $|\psi(0)\rangle = |1\rangle|0\rangle^{\otimes k}$ , decays rapidly. Conversely, if the energy gap is finite, two distinct spin dynamics can be observed, determined by PMP. If PMP occurs at  $|1\rangle$ , the survival probability stabilizes eventually at a finite value, which indicates the localization of excitation in the spin. While if not, a stretched-like dynamics was observed. This picture is a result of the competition be-



tween the energy gap, which protects excitation against the spontaneous emission into environment, and the intrinsic dissipation in the ground state function, which does not support PMP at  $|1\rangle$ .

By detecting the occurrence of energy gap and PMP at basis state  $|1\rangle$ , the critical point  $\eta_I$  or  $\eta_{II}$  can be identified, which separates the localized phase from the dissipative phase or the intermediated phase respectively. Additionally, both  $\eta_i$  and  $\eta_{II}$  display relevance to the value of  $s$ . For  $0 < s < \sim 0.6$ ,  $\eta_{II}$  is greater than  $\eta_I$ , which leads to the identification of the intermediated phase. While for  $s > \sim 0.6$ ,  $\eta_{II}$  tends to be equal to  $\eta_I$ .

The spin dynamics was also investigated in the double-excitation subspace by evaluating  $P_e(t)$  defined in Eq. (24). Interestingly, the same evolution as the survival probability in single-excitation subspace is observed. This feature would be attributed to the fact that the discretized environment corresponds to the interaction-free boson model, which enables the excitations to travel in the environment without the interference. Importantly, it is found that the bound state cannot be constructed in this case, and the dynamics of spin cannot be explained from the single-excitation perspective.

Finally, our approach would allow for an exact analysis of the effects of finite temperature on the phase transition, which is usually done by perturbational method or high-temperature approximation [20]. Further research on this topic will be presented in the future.

## ACKNOWLEDGEMENTS

H.T.C. acknowledges the support of Natural Science Foundation of Shandong Province under Grant No. ZR2021MA036. Y. A. Yan acknowledges the support of National Natural Science Foundation of China (NSFC) under Grant No. 21973036. M.Q. acknowledges the support of NSFC under Grant No. 11805092 and Natural Science Foundation of Shandong Province under Grant No. ZR2018PA012. X.X.Y. acknowledges the support of NSFC under Grant No. 12175033 and National Key R&D Program of China (No. 2021YFE0193500).

## Appendix I. SUPPLEMENTARY MATERIALS ON CDA APPROACH TO SPIN DYNAMICS IN EQ. 1

Figs. A1 illustrate explicitly evolution of the survival probability  $|\langle\psi(t)|\psi(0)\rangle|^2$  for different values of  $s$  and  $\eta$ . The solid line is decided by solving Eq. (3) with step length  $\delta t = 10^{-4}$ , and the empty circles represent results obtained by CDA. A slight difference can be observed for  $s = 1, \eta = 0.5$ . Fig. A2 illustrates the results obtain by  $\tilde{H}_{\text{dis}}$ , which shows obvious deviation from the exact results at short term evolution when  $\eta = 0.5$ .

To justify  $\tilde{H}_{\text{dis}}$ , the long-term feature of  $|\langle\psi(t)|\psi(0)\rangle|^2$  is evaluated respectively by  $\tilde{H}_{\text{dis}}$  and  $H_{\text{dis}}$ , as shown in Fig. A3. Although the convergency of calculation is rapid for  $\eta = 0.05$ , the evaluation for  $s = 0.1, 0.5$  converges slowly to a stable result with the increase of  $N$ . By the observation of convergence, it is reasonable to consider the results by  $\tilde{H}_{\text{dis}}$  as stable. This conjecture can further verified by Fig. A3 (a), in which both  $\tilde{H}_{\text{dis}}$  and  $H_{\text{dis}}$  give the same predication of spin dynamics.

However, it is admitted that the statement above is based solely on the observation in Figs. A3. Therefore,  $\tilde{H}_{\text{dis}}$  can only applicable for  $s = 1$ . For  $s = 0$  or  $0.2$ , the calculation shows that  $\tilde{H}_{\text{dis}}$  could not provide more accurate results than those by  $H_{\text{dis}}$ .

## Appendix II. SUPPLEMENTARY MATERIALS ABOUT THE QUANTUM PHASE TRANSITION IN SINGLE-EXCITATION SUBSPACE

Fig. A4 illustrates the fitting for the stretched evolution of survival probability, observed in Fig. 5 for  $\eta = 0.013, 0.026, 0.1$ . The fitting function is chosen as  $B \exp(-At^\beta)$ , in which  $A, B$  and  $\beta$  are real and non-negative. Evidently,  $\beta$  has a magnitude of order  $10^{-1}$ , and thus demonstrates clearly the stretched-like behavior.

In Fig. A5, the relevance of  $\eta_I$  and  $\eta_{II}$  to the computational parameters  $R$  and  $N$  is presented. For  $N$ , it is observed that the values of both  $\eta_I$  and  $\eta_{II}$  reach a steady state with the rise of  $N$ . However, for  $s = 1$ ,  $\eta_I$  and  $\eta_{II}$  are observed to merge into a single value close to 0.1. On the other hand, with the increase of  $R$ ,  $\eta_I$  and  $\eta_{II}$  increase very slowly for  $s = 0$  and  $s = 0.2$ . For  $s = 1$ ,  $\eta_{II}$  decreases gradually, while  $\eta_I$  stays constant. This features is a result of the fact that increase of  $R$  can improve the accuracy of computation, but is not favorable for the enhancement of efficiency.

## Appendix III. APPROACHING SPIN DYNAMICS IN DOUBLE-EXCITATION SUBSPACE BY GAUSS QUADRATURE IN REAL SPACE

In Fig. A6,  $P_e(t)$  is evaluated using Gauss quadrature method [9]. The weight function  $w(x) = (x/\omega_c)^s e^{-x/\omega_c}$  is chosen to construct the chain Hamiltonian and the number of lattice sites is set to  $N = 200$ . It is evident that  $P_e(t)$  has a similar evolution as the survival probability  $|\langle\psi(t)|\psi(0)\rangle|^2$  in single-excitation subspace. However, in contrast to CDA approach, strong fluctuations due to finite  $N$  appears when  $t > \sim 2$ , which limits the application of Gauss quadrature in the simulation of long-term dynamics in open quantum systems.

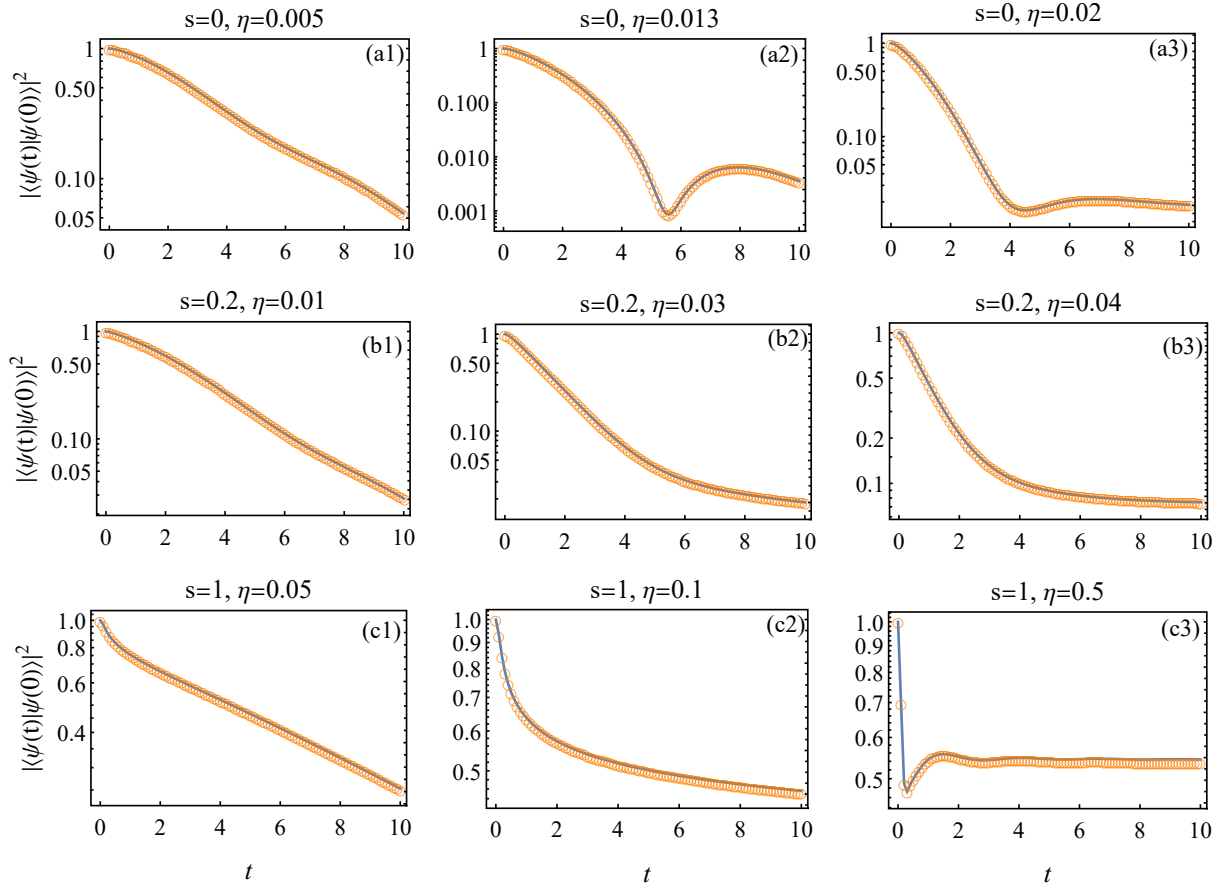


Figure A1: (Color online) The comparative plots for the survival probability  $|\langle\psi(t)|\psi(0)\rangle|^2$  with  $|\psi(0)\rangle = |e\rangle|0\rangle^{\otimes k}$  for different  $s$  and  $\eta$ . The solid line depict the exact result, whereas the empty circles represent results obtained by CDA. For all plots,  $N = 2000$ ,  $R = 6$ ,  $\Delta = 1$ , and  $\omega_c = 10$  are chosen.

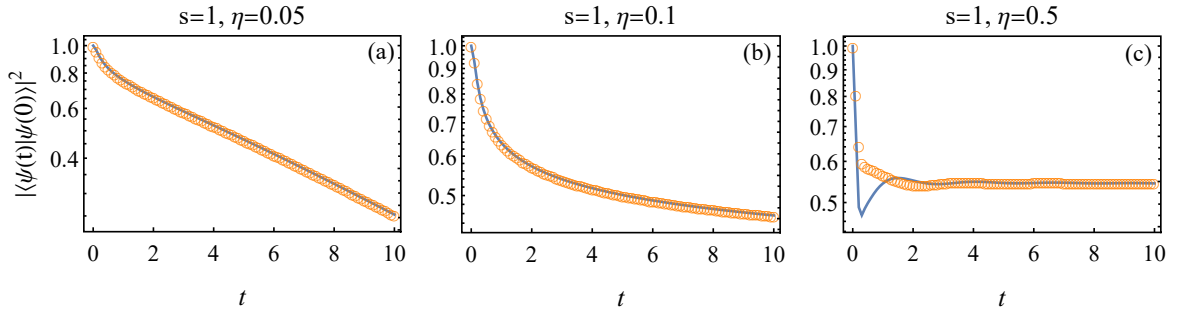


Figure A2: (Color online) The comparative plot between the exact results (solid line) and the numerics (empty circle) obtained by  $\tilde{H}_{\text{dis}}$ . The other parameters are same to those in Fig. A1.

- 
- [1] M. -J. Hwang and M. B. Plenio, *Quantum phase transition in the finite Jaynes-Cummings lattices systems*, Phys. Rev. Lett. **117**, 123602 (2016).  
[2] S. Diehl, A. Micheli, A. Kantian, B. Kraus, H. P. Büchler, and P. Zoller, *Quantum states and phases in driven open quantum systems with cold atoms*, Nat. Phys. **4**, 878-883 (2008); F. Verstraete, M. M. Wolf, and J. I. Cirac, *Quantum computation and quantum-state engineering driven by dissipation*, Nat. Phys. **5**, 633-636 (2009).  
[3] E. M. Kessler, G. Giedke, A. Imamoglu, S. F. Yelin, M. D. Lukin, and J. I. Cirac, *Dissipative phase transition in a central spin system*, Phys. Rev. A **86**, 012116 (2012).

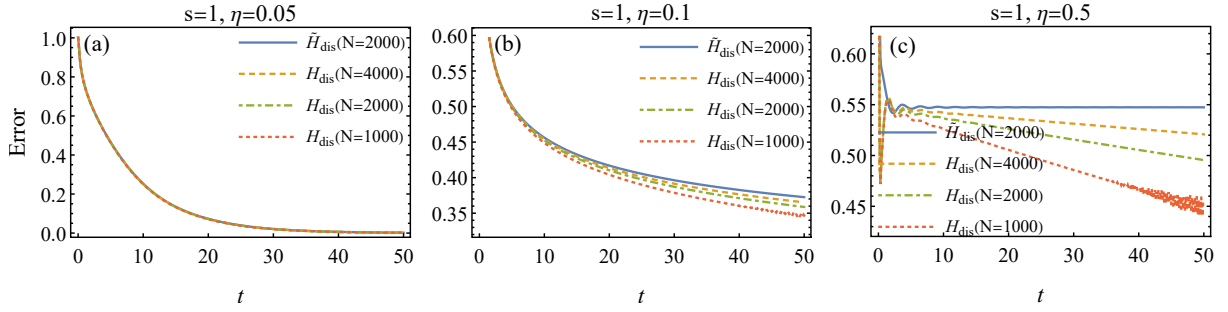


Figure A3: (Color online) Plots for CDA approach to the long-term feature of  $|\langle\psi(t)|\psi(0)\rangle|^2$  when  $\tilde{H}_{\text{dis}}$  and  $H_{\text{dis}}$  are used respectively. It is evident that the numerics by  $H_{\text{dis}}$  would become convergent to the results of  $\tilde{H}_{\text{dis}}$  when  $N$  increases.

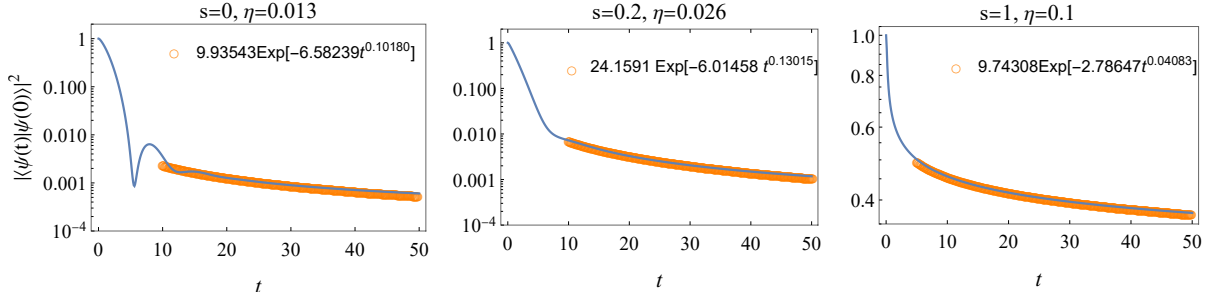


Figure A4: (Color online) The numerical fitting for the stretched-like evolution, shown in Figs. 5.

- [4] I. M. Georgescu, S. Ashhab, Franco Nori, *Quantum Simulation*, Rev. Mod. Phys. **86**, 154 (2014); M. Gong, *et.al.*, *Quantum walks on a programmable two-dimensional 62-qubit superconducting processor*, Science, **372**, 948-952 (2021); Q. Zhu, *et.al.*, *Quantum computational advantage via 60-qubit 24-cycle random circuit sampling*, Science Bulletin, **67**(3), 240-245 (2022).
- [5] A. F. Kockum, A. Miranowicz, S. De Liberato, S. Savasta and F. Nori, *Ultrastrong coupling between light and matter*, Nat. Rev. Phys. **1**, 19-40 (2019); P. Forn-Díaz, L. Lamata, E. Rico, J. Kono, and E. Solano, *Ultrastrong coupling regimes of light-matter interaction*, Rev. Mod. Phys. **91**, 025005.
- [6] I. de Vega, D. Alonso, *Dynamics of non-Markovian open quantum systems*, Rev. Mod. Phys. **89**, 015001 (2017); H. Weimer, A. Kshetriyayum, R. Orús, *Simulation methods for open quantum many-body systems*, Rev. Mod. Phys. **93**, 015008 (2021).
- [7] H. P. Breuer, F. Petruccione, *The Theory of Open Quantum Systems*, Oxford University Press (2002).
- [8] R. S. Burkey, C. D. Cantrell, *Discretization in the quasi-continuum*, J. Opt. Soc. Am. B **1**, 169-175 (1984); A. K. Kazansky, *Precise analysis of resonance decay law in atomic physics*, J. Phys. B: At. Mol. Opt. Phys. **30**, 1404-1410 (1997); H. P. Breuer, J. Gemmer, M. Michel, *Non-Markovian quantum dynamics: correlated projection superoperators and Hilbert space average*, Phys. Rev. A **73**, 016139 (2006); H. P. Breuer, *Non-Markovian generalization of the Lindblad theory of open quantum systems*, Phys. Rev. A **75**, 022103 (2007); N. Shenvi, J. R. Schmidt, S. T. Edwards, and J. C. Tully, *Efficient discretization of the continuum through complex contour deformation*, Phys. Rev. A **78**, 022502 (2008); Haobing Wang and M. Thoss, *From coherent motion to localization: dynamics of the spin-boson model at zero temperature*, New J. Phys. **10**, 115005 (2008).
- [9] A. W. Chin, Á. Rivas, S. F. Huelga, and M. B. Plenio, *Exact mapping between system-reservoir quantum models and semi-infinite discrete chains using orthogonal polynomials*, J. Math. Phys. **51**, 092109 (2010).
- [10] H. T. Cui, Y. A. Yan, M. Qin, and X. X. Yi, *Complex discretization approximation for the full dynamics of system-environment quantum models*, arXiv: 2303.06584 [quant-ph] (2023).
- [11] A. J. Leggett, S. Chakravarty, A. T. Dorsey, Matthew P. A. Fisher, A. Garg, and W. Zwerger, *Dynamics of the dissipative two-state system*, Rev. Mod. Phys. **59**, 1-85 (1987); U. Weiss, *Quantum Dissipative Systems* (World Scientific, Singapore, 1999).
- [12] R. Bulla, N.-H. Tong, and M. Vojta, *Numerical renormalization group for bosonic systems and applications to the sub-Ohmic spin-boson model*, Phys. Rev. Lett. **91**, 170601 (2003); F. B. Anders, R. Bulla, and M. Vojta, *Equilibrium and nonequilibrium dynamics of the sub-Ohmic spin-boson model*, Phys. Rev. Lett. **98**, 210402 (2007); A. Winter, H. Rieger, M. Vojta, and R. Bulla, *Quantum phase transition in the sub-Ohmic spin-boson model: quantum Monte Carlo study with a continuous imaginary time cluster algorithm*, Phys. Rev. Lett. **102**, 030601 (2009); A. Alvermann and H. Fehske, *Sparse polynomial space approach to dissipative quantum systems: application to the sub-Ohmic spin-boson model*, Phys. Rev. Lett. **102**, 150601 (2009); A. W. Chin, J. Prior, S. F. Huelga, and M. B. Plenio, *Generalized polaron ansatz for the ground state of the sub-Ohmic spin-boson model: an analytic theory of the localization transition*, Phys.

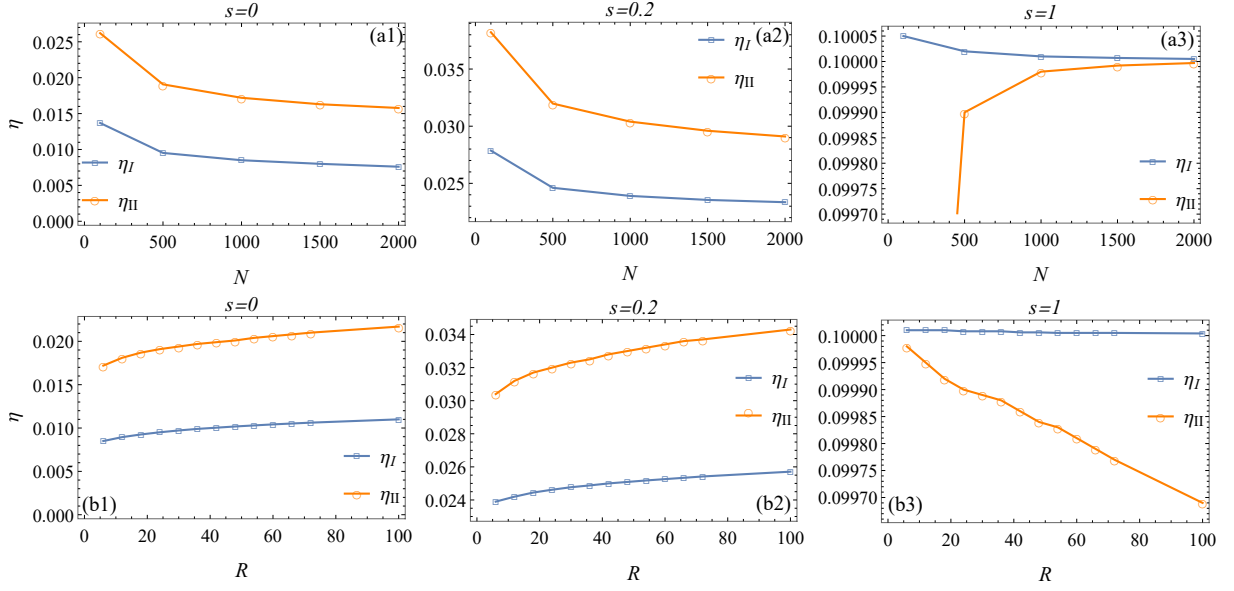


Figure A5: (Color online)  $\eta_I$  and  $\eta_{II}$  vs. the parameter  $R$  and  $N$ . For panels (a1)-(a3),  $R = 6$  is chosen. While for panels (b1)-(b3),  $N = 1000$  is chosen. For all plots,  $\Delta = 1, \omega_c = 10$  are chosen.

- Rev. Lett. **107**, 160601 (2011); A. Stratheran, P. Kirton, D. Kilda, J. Keeling, and B. W. Lovett, *Efficient non-Markovian quantum dynamics using time-evolving matrix product operators*, Nat. Commun. **9**, 3322 (2018); F. Otterpohl, P. Nalbach, and M. Thorwart, *The hidden phase of the spin-boson model*, Phys. Rev. Lett. **129**, 120406 (2022).
- [13] Yan-Zhi Wang, Shu He, Liwei Duan, and Qing-Hu Chen, *Quantum phase transition in the spin-boson model without counterrotating terms*, Phys. Rev. B **100**, 115106 (2016).
- [14] A. G. Kofman, G. Kurizki, and B. Sherman, *Spontaneous and induced atomic decay in photonic band structures*, J. Mod. Opt. **41**, 353-384 (1994).
- [15] Q.-J. Tong, J.-H. An, H.-G. Luo, and C. H. Oh, *Mechanism of entanglement preservation*, Phys. Rev. A **81**, 052330 (2010); H.-N. Xiong, W.-M. Zhang, Xiaoguang Wang, and M.-H. Wu, *Exact non-Markovian cavity dynamics strongly coupled a reservoir*, Phys. Rev. A **82**, 012105 (2010); Q.-J. Tong, J.-H. An, H.-G. Luo, and C. H. Oh, *Quantum phase transition in the delocalized regime of the spin-boson model*, Phys. Rev. B **84**, 174301 (2011).
- [16] Tao Shi, Ying-Hai Wu, A. González-Tudela, and J. I. Cirac, *Bound states in Boson Impurity Models*, Phys. Rev. X **6**, 021027 (2016).
- [17] R. Bulla, Th. Pruschke, and A. C. Hewson, *Anderson impurity in pseudo-gap Fermi systems*, J. Phys. Condens. Matter **9**, 10463-10474 (1997).
- [18] W. Gautschi, G. V. Milovanović, *Polynomials orthogonal on the Semicircle*, J. Approx. Theo. **46**, 230-250 (1986); W. Gautschi, H. J. Landau, and G. V. Milovanović, *Polynomials orthogonal on the Semicircle II*, Constr. Approx. **3**, 389-404 (1987).
- [19] S. Sachdev, *Quantum Phase transition* (Cambridge University Press, Cambridge, 2011).
- [20] D. Tamascelli, A. Smirne, J. Lim, S. F. Huelga, and M. B. Plenio, *Efficient simulation of finite-temperature open quantum systems*, Phys. Rev. Lett. **123**, 090402 (2019).
- [21] Dorje C Brody, *Biorthogonal quantum mechanics*, J. Phys. A: Math. Theor. **47**, 035305 (2014).

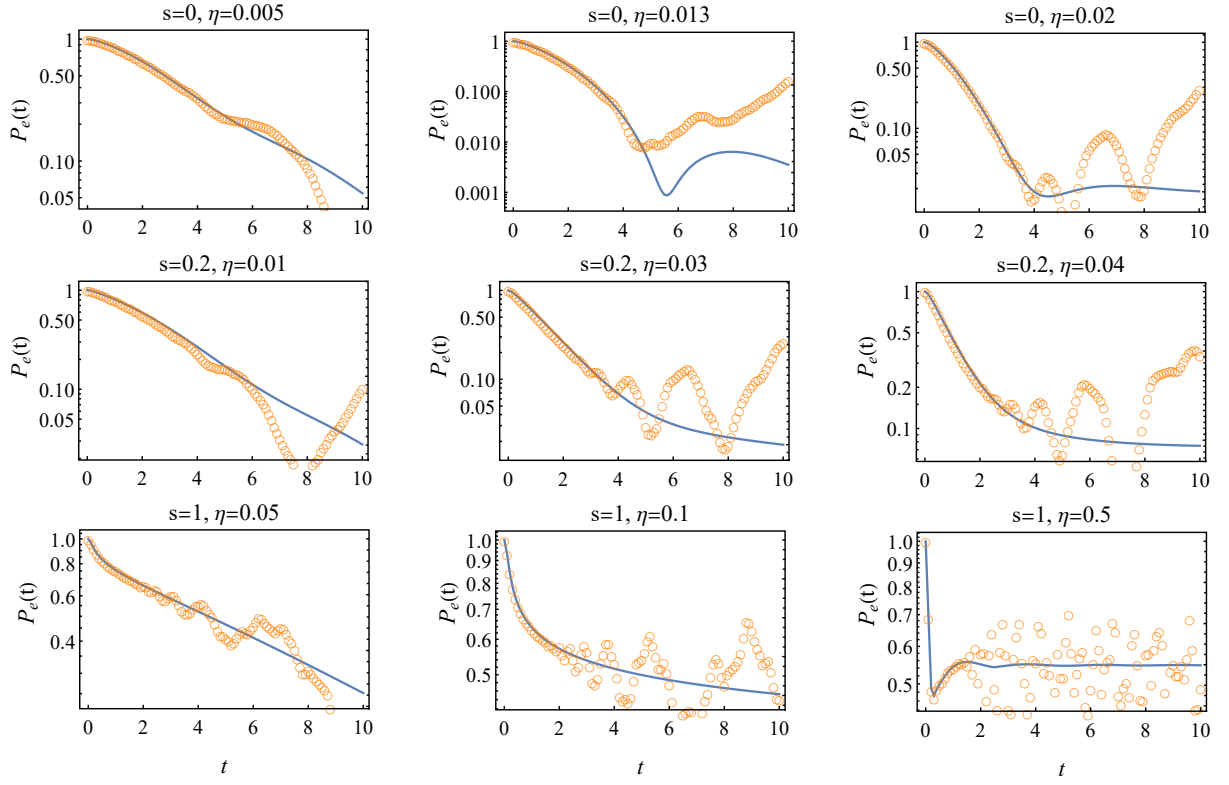


Figure A6: (Color online) The reevaluation of spin dynamics in the double-excitation subspace (empty circle) by Gauss quadratures method. The solid line corresponds to the result of  $|\langle\psi(t)|\psi(0)\rangle|^2$  in single-excitation subspace. For all plots,  $\Delta = 1$  and  $\omega_c = 10$  are chosen.